Tunneling and hopping conduction via localized states in thin $PrBa_2Cu_3O_{7-x}$ barriers

J. Yoshida and T. Nagano
Advanced Research Laboratory, Toshiba Corporation, 1, Komukai Toshiba-cho, Sarwai-ku, Kawasaki 210, Japan
(Received 9 January 1997)

The mechanism of current transportation across $PrBa_2Cu_3O_{7-x}$ thin films was investigated for a,b-axis oriented Au/$PrBa_2Cu_3O_{7-x}$/$YBa_2Cu_3O_{7-x}$ junctions with a $PrBa_2Cu_3O_{7-x}$ barrier layer ranging from 5 to 30 nm in thickness. Resonant tunneling and hopping conduction via a small number of localized states were confirmed through the observation of characteristic power-law dependence of junction conductance on both temperature and voltage at low temperatures. The radius and the density of the localized states in thin $PrBa_2Cu_3O_{7-x}$ barrier layers were estimated to be 1.1 nm and 5.0×10^{19} eV^{-1} cm^{-3}, respectively. The conductance of a junction with a 7.5-nm thick barrier at 1.7 K did not exhibit any decrease in a magnetic field of up to 6 T, indicating either that on-site Coulomb repulsion of electrons in the localized states is anomalously weak or that magnetic coupling between singly occupied localized states suppresses the Coulomb correlation effect on resonant tunneling. [S0163-1829(97)16117-3]

I. INTRODUCTION

One of the most promising applications of high-temperature superconductive devices is an ultrafast digital circuit utilizing a single magnetic flux quantum as an information carrier. Single-flux-quantum circuits using conventional Nb Josephson junctions with I_cR_n product values of around 0.2 mV have already been demonstrated to work at clock frequencies exceeding 100 GHz. If Josephson junctions with higher I_cR_n product values can be developed using high-temperature superconductors, a significant increase in the operation frequency as well as a higher operation temperature compared to Nb technology will become possible.

The absence of superconductivity and semi-insulative behavior in $PrBa_2Cu_3O_{7-x}$ (PBCO) make the material an attractive candidate for an artificial barrier in Josephson junctions with $YBa_2Cu_3O_{7-x}$ (YBCO) superconductive electrodes. Although a nearly ideal Josephson effect in YBCO/PBCO/YBCO junctions has been demonstrated by several groups,[2–7] no conventional theory based on either tunneling or the proximity effect has given a satisfactory explanation for the mechanism of Josephson coupling through the considerably thick PBCO barrier layers amounting to several tens of nm. Recently, resonant tunneling of Cooper pairs through localized states with long localization length has been proposed as a possible origin of Josephson coupling in these junctions.[6–10] These localized states are believed to be associated with the CuO chains in PBCO, for which a unique electronic structure has been predicted theoretically[11] and confirmed experimentally.[12,13] Experimental confirmations of resonant tunneling of Cooper pairs via localized states in PBCO have been reported by several groups for junctions with a ramp-edge geometry.[6,7,10] However, more recent work on both PBCO barrier junctions and Ga-doped PBCO barrier junctions seems to deny the possibility.[14] An alternative explanation for the Josephson coupling based on the proximity effect in the CuO chains in which metallic conduction paths remain at least locally even at low temperatures has been proposed by Lee *et al.*[15] Furthermore, some evidence of local superconductivity in PBCO has been reported by Blackstead *et al.*[16]

Our previous study of YBCO/PBCO/YBCO junctions with a PBCO barrier thicker than 20 nm has revealed that both tunneling paths and hopping paths coexist within the barrier layer.[17] However, no definite evidence of current transport via a small number or localized states or remaining metallic conduction paths has been confirmed. We have extended our research to Au/PBCO/YBCO junctions in order to obtain further information on the transport mechanism as well as on the localized states in very thin PBCO layers. The reason that we used Au/PBCO/YBCO junctions instead of YBCO/PBCO/YBCO junctions is as follows. In the case of YBCO/PBCO/YBCO junctions, if one small microshort which can carry superconducting current exists within the junction, the junction characteristics are governed completely by the properties of the microshort. This has made it impossible to derive information concerning the very thin PBCO barrier layer itself. On the other hand, in the case of Au/PBCO/YBCO junctions, possible microshorts between Au and YBCO are known to exhibit a contact resistance of the order of 10^{-8} Ω cm^2.[18] Therefore, if the effective area of the microshort is not particularly large, we can neglect the contribution of microshorts to the junction conductance. In fact, we have been able to observe a systematic dependence of junction conductance on the barrier layer thickness for Au/PBCO/YBCO junctions with a PBCO barrier down to 5 nm, as will be discussed in the subsequent sections.

In this paper, we report the results of a detailed study of current transport in a,b-axis oriented Au/PBCO/YBCO junctions and discuss the physical nature of the localized states in PBCO and its relevance to transport properties. Attention is also paid to the possibility of resonant tunneling of Cooper pairs via localized states in PBCO barriers.

II. EXPERIMENTAL PROCEDURE

PBCO/YBCO bilayer films were grown on $SrTiO_3(100)$ substrates using a multitarget sputtering system equipped with Y, Pr, Cu, and BaCu alloy targets. The power supplied

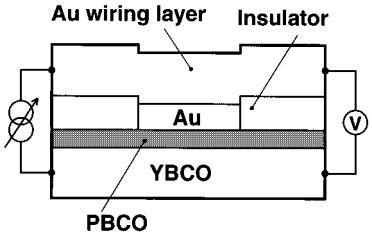

FIG. 1. Schematic representation of Au/PBCO/YBCO junction structure.

to individual targets was controlled precisely to maintain the film composition at the stoichiometric value with a deviation of less than 3%. A 50% O_2-containing Ar/O_2 gas was introduced into the chamber at a pressure of 1.2 Pa, and the substrate temperature was fixed at 620 °C. We have developed a method of preparing YBCO films with a complete *a*-axis orientation based on the use of buffer layers composed of 123 materials with cubic symmetry.[19] These cubic compounds with a simple perovskite structure were found to grow selectivity on a $SrTiO_3(100)$ surface within a relatively narrow window of substrate temperature and growth rate. Atomic force microscope (AFM) studies confirmed that the maximum surface roughness of a 250-nm thick YBCO film on the buffer was around 2 nm. Careful x-ray studies of PBCO/YBCO bilayer films revealed that although the bottom YBCO layer maintained a complete *a*-axis orientation, the PBCO layer on it grew with a predominantly *b*-axis orientation, i.e., with the CuO chains normal to the film surface. A *b*-axis orientation of PBCO on an *a*-axis oriented YBCO film is reasonable from the viewpoint of lattice matching between these two materials. The surface coverage of YBCO by a thin PBCO film was investigated using a secondary ion mass spectroscopy (SIMS) profiling technique. We were not able to observe the signal from Y ions on a 10-nm thick PBCO layer surface. This indicates better than 99.9% coverage of the YBCO film surface even by a 10-nm thick PBCO layer.

Figure 1 shows the junction structure which we used for the transport measurements. The thickness of the bottom YBCO layer was 250 nm and the PBCO barrier layer thickness was varied from 5 to 30 nm. The junction fabrication process started with the deposition of 100-nm thick Au onto the bilayers in another vacuum chamber immediately after taking out the bilayers from the sputtering machine. Possible damage of the bilayer film surface during this *ex situ* process was investigated by comparing Josephson characteristics of Pb/Ag/Au/YBCO junctions prepared by the *ex situ* method to those fabricated by an *in situ* method.[17] We were not able to find a significant difference between these two types of junctions in both a Josephson critical current density and a junction resistance. Junction dimensions ranging from 20 $\times 20$ μm^2 to 100×100 μm^2 were defined by a photolithography process followed by etching the Au layer by an aqueous solution of KI and I. After providing an isolation layer with a negative resist, 1-μm thick Au wiring layer was deposited through a metal mask. Five junctions having different junction areas were fabricated in one chip, while two chips were simultaneously defined on one wafer. The junctions on one wafer exhibited junction conductances which were scaled well with the areas.

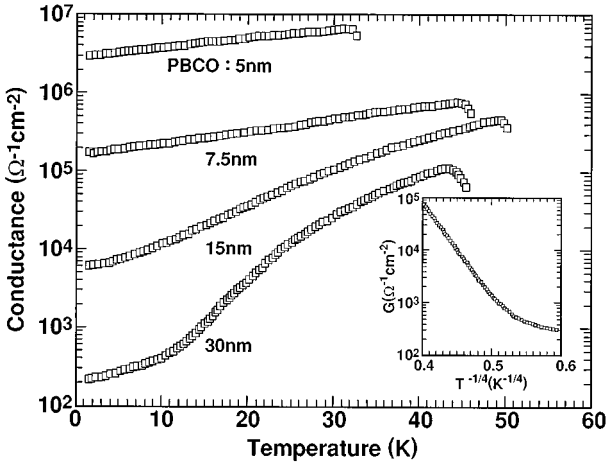

FIG. 2. Temperature dependence of zero-voltage conductance observed for Au/PBCO/YBCO junctions with a PBCO barrier ranging from 5 to 30 nm. The inset shows the semilog plot of the conductance of a 30-nm thick barrier junction as a function of $T^{-1/4}$.

An ac technique with a voltage modulation amplitude well below 100 μV was used to measure the zero-voltage conductance as a function of temperature in the temperature range of 1.4 K to the critical temperature of the YBCO electrodes. A similar technique was also used to obtain differential conductance versus voltage characteristics.

III. EXPERIMENTAL RESULTS AND DISCUSSION

A. Temperature dependence of junction conductance

Figure 2 shows the temperature dependence of zero-voltage conductance G for junctions with a PBCO layer ranging from 5 to 30 nm in thickness. The junction conductance at low temperatures can be seen to increase almost exponentially with decreasing the PBCO layer thickness. Furthermore, the temperature dependence becomes weaker with a decrease in the PBCO layer thickness. In the case of a 5-nm thick PBCO barrier junction, the junction conductance was found to exhibit a simple power law dependence on temperature with the form

$$G(T)=G_0+\alpha T^{4/3}, \tag{1}$$

where G_0 denotes the temperature-independent conductance, T is the temperature, and α is an adjustable parameter, as shown in Fig. 3. Such a dependence is exactly what is expected for a tunnel junction in which both an elastic process and inelastic hopping of electrons via a pair of localized states contribute to the current conduction.[20] In contrast, the behavior of the junction with a 30-nm thick barrier above 20 K seems to follow the variable range hopping conduction which is a percolative process via a large number of localized states, as seen in the inset in Fig. 2 where the junction conductance is plotted on a logarithmic scale as a function of $T^{-1/4}$. These preliminary analyses of the data in Fig. 2 demonstrate that a crossover from tunneling to variable range hopping in semi-insulative PBCO barriers occurs within the thickness and temperature range which we are investigating.

It is well recognized that when the thickness of an insulative barrier with localized states is not much thicker than

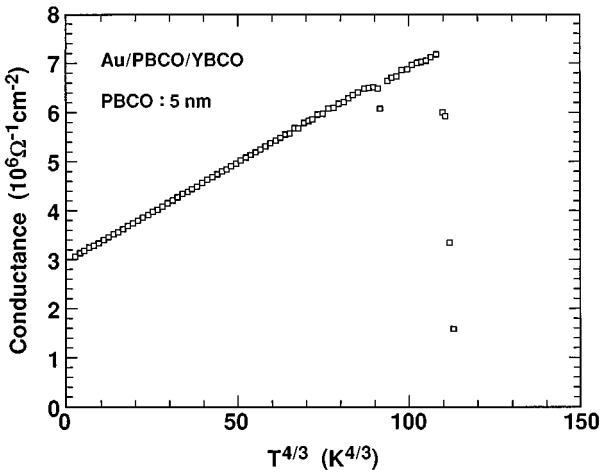

FIG. 3. Plot of the zero-voltage conductance G as the function of the 4/3 power of temperature T. Linear relationship between G and $T^{4/3}$ is clearly seen in the temperature range from 1.4 K to the critical temperature of the YBCO electrode, indicating that the conductance can be expressed as $G(T)=G_0+\alpha T^{4/3}$, where G_0 and α are constants being independent of temperature.

the radius (localization length) of the localized states, the current conduction across the barrier is governed by direct tunneling of electrons between two electrodes. As the barrier thickness increases, resonant tunneling via a localized state comes to give a higher conductance than the direct tunneling process.[21] According to a simple one-dimensional model for resonant tunneling, in which the effect of intra-atomic Coulomb interaction between electrons at the resonant state is neglected, the junction conductance in unit area averaged over the positions and energies of the localized states in the barrier is given by[22]

$$G_{\rm res}=\frac{\pi e^2}{\hbar}\, gaE_0\exp(-d/a)=\frac{\pi e^2}{\hbar}\, ga\Gamma, \tag{2}$$

where g and a are the density and the radius of the localized state, E_0 is a measure of the effective depth of the localized state, and d is the thickness of the barrier. $\Gamma[=E_0\exp(-d/a)]$ on the right-hand side of the equation denotes the effective width in energy of the resonant state.

Further increase in barrier layer thickness results in opening of new conduction channels in which two or more consecutive localized states play a definite role. Glazman and Matveev have derived general formulas which can describe hopping conduction processes via a small number of localized states in a moderately thick insulative barrier.[20] According to the theory, in the case that the number of localized states involved in current conduction is two, the highest conductance path is realized by an elastic transfer of electrons into the first localized state from the left electrode followed by hopping to the second state with the emission or the absorption of a phonon and then tunneling out to the right electrode. Under the assumption that the hopping process between two localized states is governed by the interaction with acoustic phonons with a linear dispersion relation, the junction conductance at zero voltage can be expressed as

$$G_2(T)=\nu_{2T}\,\frac{e^2}{\hbar}\, g^2E_0^{2/3}\lambda^{1/3}(k_BT)^{4/3}a^3d\,\exp\!\left(-\frac{2d}{3a}\right), \tag{3}$$

where ν_{2T} is a numerical parameter and λ is a dimensionless quantity which describes the strength of electron-phonon coupling at the localized state, of which the explicit expression is given using the average deformation potential Λ, the mass density of the barrier ρ, and the sound velocity v_s as

$$\lambda=\frac{\Lambda^2E_0^2}{\hbar^3\rho v_s^5}. \tag{4}$$

Equation (3) indicates that the inelastic process via two localized states exhibits a characteristic power law dependence of junction conductance on temperature as $T^{4/3}$ as well as a weaker thickness dependence compared with that in resonant tunneling conduction. This characteristic power law dependence is exactly what we have seen in Fig. 3.

The number of localized states which take part in current conduction across a semi-insulative barrier increases with an increase in the barrier layer thickness, density of the localized states, or temperature. The general expression for the hopping conductance due to conduction channels consisting of n localized states is given by Glazman and Matveev as

$$\begin{aligned}G_n(T)=\nu_{nT}\,\frac{e^2}{\hbar}\, g^nE_0^{2/(n+1)}\lambda^{(n-1)/(n+1)}&\\ \times(k_BT)^{(n^2+n-2)/(n+1)}a^{2n-1}d^{n-1}&\\ \times\exp\!\left(-\frac{2d}{(n+1)a}\right),&\end{aligned} \tag{5}$$

where ν_{nT} is a numerical parameter. It is evident from the equation that a higher order power law dependence on temperature appears with an increase in the number of localized states involved in the conduction channels being accompanied with a weaker exponential dependence on the barrier layer thickness. This suggests that the most dominating conduction channel in a junction depends on the barrier layer thickness, the density of localized states, and temperature.

The total conductance of a junction at any temperature is given by the sum of the contributions from all the channels, that is

$$G(T)=G_{\rm dir}+G_{\rm res}+\sum_{n\geqslant 2}G_n(T), \tag{6}$$

where $G_{\rm dir}$ describes the conductance due to direct tunneling, and $G_{\rm dir}$ and $G_{\rm res}$ are considered to be independent of temperature in the first order approximation.[23] It is easy to see from Eq. (5) that in the temperature range

$$T_n<T<T_{n+1}, \tag{7}$$

the term $G_n(T)$ in Eq. (6) dominates the current conduction, where T_n is given by

$$\begin{aligned}T_n=\left(\frac{\nu_{nT}}{\nu_{(n-1)T}}\,k_Bga^2d\right)^{-1}&\left[\frac{\nu_{nT}}{\nu_{(n-1)T}}\,g\,\frac{E_0}{\lambda}\,a^2d\right.\\ &\left.\times\exp\!\left(-\frac{d}{a}\right)\right]^{2/(n^2+n+2)}.\end{aligned} \tag{8}$$

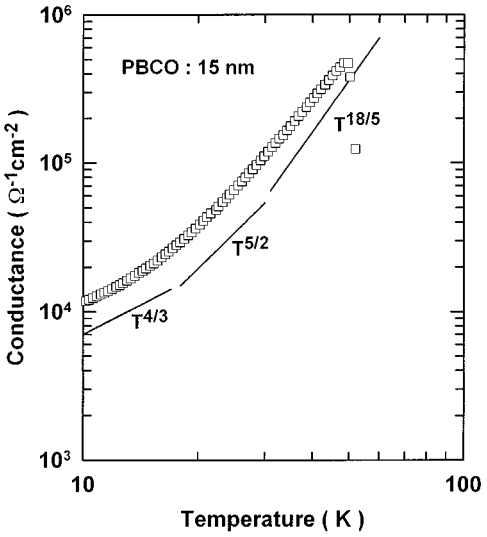

FIG. 4. Zero-voltage conductance versus temperature for a junction with a 15-nm thick PBCO barrier plotted in log-log scale. The slope of the curve increases with an increase in temperature and the steepest slope lies between 5/2 and 18/5, implying that the data can be fit by Eq. (6) with $n \leqslant 4$.

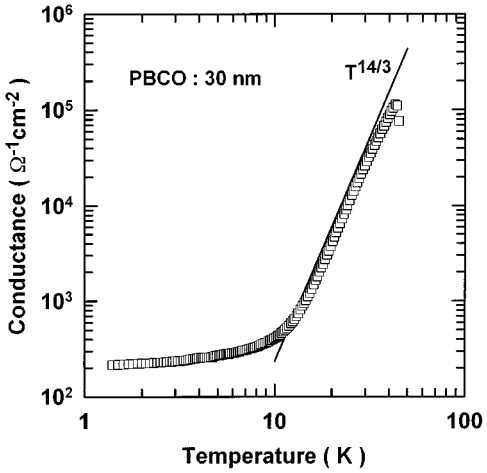

FIG. 5. The log-log plot of the conductance versus temperature characteristic for a junction with a 30-nm thick PBCO barrier. The slope of the curve increases with increasing the temperature, approaching the maximum value of 14/3 at around 20 K, and then it decreases at higher temperatures. This indicates that Eq. (6) is insufficient to fit the data.

We first tried to analyze the data in Fig. 2 using Eq. (6). The first step of the analysis was to determine the maximum n value in Eq. (6) which was required to reproduce the experimental data for each junction. This was done by plotting the conductance versus temperature characteristic in log-log scale. One example of the plot is shown in Fig. 4 for a junction with a 15-nm thick PBCO barrier. It is apparent that the maximum slope of the plotted curve falls between 5/2 and 18/5, implying that the number of the localized states involved in the current transport in the junction is less than 4. Unfortunately, however, such a procedure did not work well for junctions with a PBCO barrier layer thicker than 20 nm. The log-log plot of the conductance versus temperature characteristic of a junction with a 30-nm thick barrier is shown in Fig. 5. The slope of the curve in Fig. 5 increases with increasing temperature, approaching 14/3 at around 20 K, and then it decreases at higher temperatures. Such a behavior is never expected from Eq. (6), indicating that Eq. (6) is insufficient to reproduce the experimental data for a junction with a thick PBCO barrier layer. One striking feature of the junctions of which the temperature dependence of conductance cannot be described well by Eq. (6) is that a variable range hopping model seems to give a better description of the behavior at high temperatures, as seen in the inset in Fig. 2. Based on this finding, we added a variable range hopping term to Eq. (6) to analyze the data for junctions with a PBCO barrier thicker than 20 nm:

$$G(T)=G_{\mathrm{dir}}+G_{\mathrm{res}}+\sum_{n\geqslant 2} G_n(T)+\sigma_0 d^{-1}\exp(-(T_0/T)^{1/4}), \tag{9}$$

where T_0 is given by

$$k_B T_0 = 21/g a^3. \tag{10}$$

When Eq. (9) was used to analyze the experimental data, we first estimated the values of $\sigma_0 d^{-1}$ and T_0 from a logarithmic plot of the junction conductance against $T^{-1/4}$. Then, after subtracting the contribution of the variable range hopping term from the experimental data, we determined the maximum n value in Eq. (9) according to the procedure already described.

The preliminary analysis described above led us to fit the data in Fig. 2 to the form

$$G=G_0+\alpha T^{4/3}+\beta T^{5/2}+\gamma T^{18/5}+\sigma_0 d^{-1}\exp(-(T_0/T)^{1/4}), \tag{11}$$

where G_0 denotes a temperature-independent term originating from both direct and resonant tunneling, and α, β, and γ are fitting parameters. The last term on the right-hand side of Eq. (11) was incorporated only for junctions with a PBCO layer thicker than 20 nm and σ_0 and T_0 were dealt with as predetermined parameters in the course of least squares fitting to determine other parameters. Table I summarizes the parameters obtained by the fit. The temperature dependence of junction conductance calculated from Table I is shown in Fig. 6. The excellent agreement between Fig. 2 and Fig. 6 confirms that tunneling and hopping conduction via a small number of localized states govern the current transport across the PBCO barrier layers in our junctions at least at low temperatures. The hopping conduction via a small number of localized states crosses over fairly abruptly to variable range hopping at around 30 K injunctions with a PBCO barrier layer exceeding 20 nm in thickness. A similar behavior has been reported for the current conduction across a thin amorphous silicon barrier when the barrier layer thickness exceeds the typical hopping length l_{VRH}:[24]

$$l_{\mathrm{VRH}}=a(T_0/T)^{1/4} \tag{12}$$

l_{VRH} in our junctions can be calculated to be about 21 nm at 25 K from T_0 in Table I and a which will be estimated in the next section. This value corresponds well with the crossover point which was observed experimentally for our junctions.

TABLE I. Parameters for Eq. (11) obtained by the fits to the experimental conductance versus temperature characteristics shown in Fig. 2.

d (nm)	G_0 (Ω^{-1} cm^{-2})	α (Ω^{-1} cm^{-2} K$^{-4/3}$)	β (Ω^{-1} cm^{-2} K$^{-5/2}$)	γ (Ω^{-1} cm^{-2} K$^{-18/5}$)	σ_0 (Ω^{-1} cm^{-1})	T_0 (K)
5	2.9×10^{6}	4.0×10^{4}				
7.5	1.8×10^{5}	2.2×10^{3}	2.2×10^{1}			
10	4.8×10^{4}	1.2×10^{3}	9.8×10^{1}			
15	5.9×10^{3}	1.2×10^{2}	5.6×10^{0}	3.2×10^{-1}		
20	7.3×10^{2}	2.2×10^{1}	1.2×10^{0}	1.5×10^{-1}	1.9×10^{7}	3.3×10^{6}
30	2.1×10^{2}	6.0×10^{0}	2.0×10^{-3}		9.7×10^{6}	3.7×10^{6}

B. Evaluation of physical parameters of localized states in PBCO

Equation (5) indicates that the hopping conductance due to a channel involving n localized states exhibits a characteristic exponential dependence on barrier layer thickness d

$$G_n \propto d^{n-1}\exp\left(-\frac{2d}{(n+1)a}\right). \tag{13}$$

This dependence enables us to determine the radius of the localized state a from the data listed in Table I. It should be noted, however, that we should be cautious in treating the G_0 term in Table I, because this term can contain in principle the contributions from both direct and resonant tunneling, each of which possesses its own thickness dependence. Taking this point into account, we first analyze the behavior of α which is the coefficient of the $T^{4/3}$ term in the total conductance. Figure 7 shows the semilog plot of α/d versus d. Except for the data for junctions with a 30-nm thick barrier, we can see a nearly linear dependence. From the slope of the line in Fig. 7 and Eq. (13), the radius of the localized states in PBCO is estimated to be 1.1 nm. Keeping this value in mind, let us look at the data for G_0 in Fig. 8. Although G_0 does not exhibit a simple exponential dependence on d especially when d exceeds 15 nm, it is apparent that the steepest slope which appears in the log G_0 versus d plot is $1/a$. This fact implies that the temperature independent conductance in our junctions is not governed by direct tunneling but by resonant tunneling. Then, the question is what causes the deviation of the data in Fig. 8 from a straight line. The simplest explanation may be the inhomogeneity in the barrier layer thickness which increases with an increase in d. It is highly probable that the contribution to the total junction conductance from a local conduction path in which the PBCO layer thickness is accidentally thin becomes notable with increasing the nominal barrier layer thickness. However, we have not been able to detect a significant deterioration of the surface morphology of PBCO/YBCO bilayer films associated with an increase in the film thickness even by AFM observations. Another possibility to be considered is an asymmetric barrier structure originating inherently from the Au/PBCO/YBCO structure of our junctions. It is easy to conceive that some builtin electric field appears within the PBCO barrier due to the difference in work functions between Au and YBCO or the difference in the interface structures. In fact, we usually observe weak asymmetry in the differential conductance versus voltage characteristic of our junctions with the inversion of the bias polarity. The exact treatment of this asymmetric barrier problem, however, re-

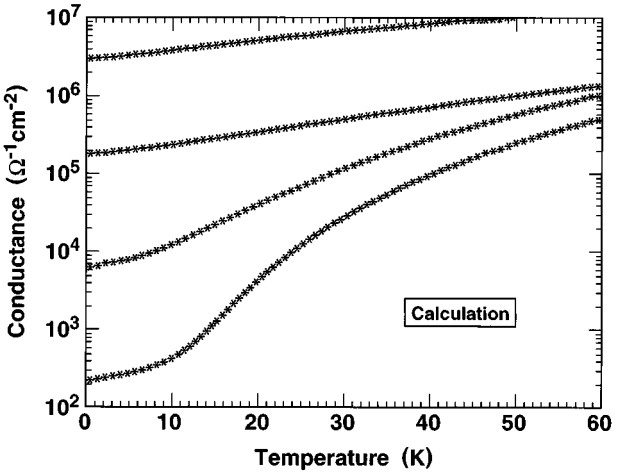

FIG. 6. Theoretical temperature dependence of junction conductance calculated by Eq. (11) and numerical parameters listed in Table I. Each curve in the figure corresponds to the experimental data for junctions with a PBCO barrier of various thickness shown in Fig. 2.

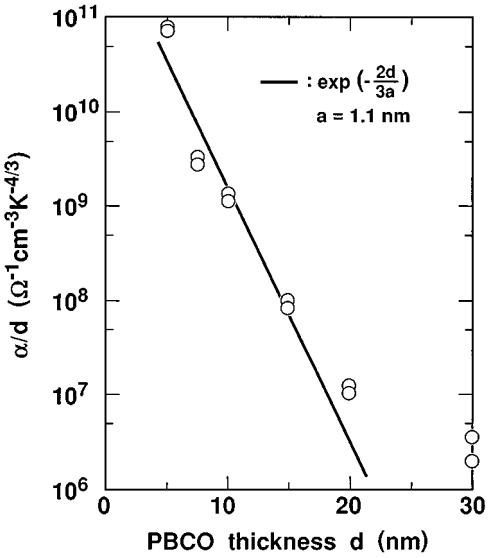

FIG. 7. Plot of the coefficient of the $T^{4/3}$ term of junction conductance as a function of the barrier layer thickness. The solid line indicates the relation expected for the hopping conduction via two localized states with a radius of 1.1 nm.

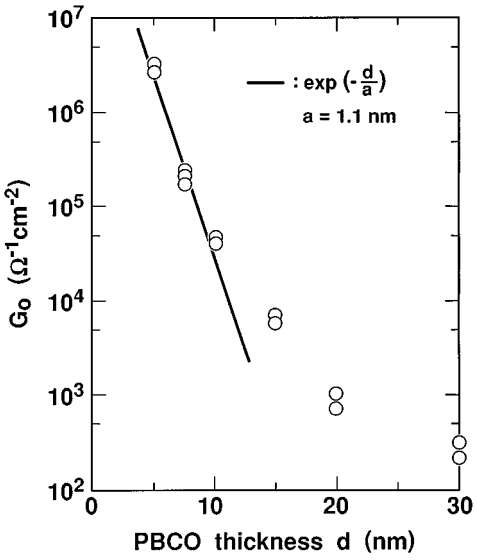

FIG. 8. Plot of the temperature independent conductance G_0 as a function of the barrier layer thickness. Although G_0 does not exhibit a simple exponential dependence on the barrier thickness, the steepest slope which appears in the plot coincides well with that expected for resonant tunneling via a localized state with a radius of 1.1 nm.

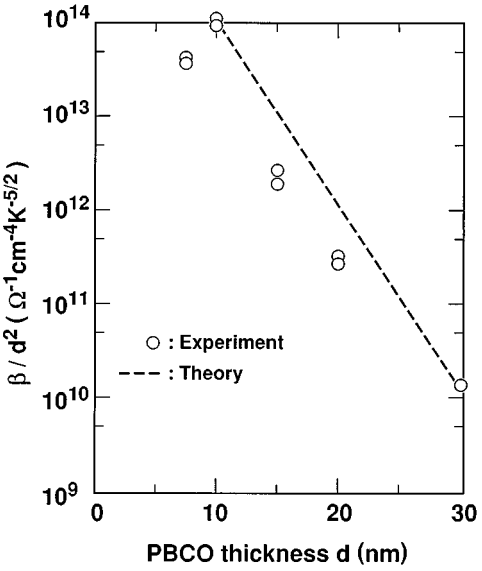

FIG. 9. Comparison between experimentally determined coefficients of the $T^{5/2}$ term in junction conductance (open circles) and theoretical calculation (dashed line) using Eq. (5) and physical parameters for the localized states in PBCO listed in Table II.

quires detailed information on the potential shape in actual junctions. Unfortunately, we do not have data sufficient to discuss the problem further. Accordingly, we proceed to the following discussions by assuming that we can regard the potential barrier as a symmetric one unless the PBCO layer thickness is not particularly large.

The current transport across a thin insulative barrier containing localized states can be described quantitatively by four physical parameters, a, g, E_0, and λ, as seen in Eqs. (2) and (5). Among the parameters, a has already been determined to be 1.1 nm from the thickness dependence of α. It is straightforward to derive the density of the localized state g from the characteristic temperature T_0 of the variable range hopping conduction observed for our junctions with a PBCO barrier thicker than 20 nm. When we adopt the value for a 30-nm barrier junction in Table I, g is calculated to be 5.0×10^{19} eV^{-1} cm^{-3} from Eq. (10). Since resonant tunneling is an elastic process, the conductance due to it does not depend on the electron-phonon coupling parameter λ, as seen in Eq. (2). By using this fact, we can determine the effective depth of the localized state E_0 from the y intercept of the line in Fig. 8. The remaining parameter λ can be calculated from the y intercept of the line in Fig. 7 using Eq. (3) and the values of other parameters obtained by the procedure described above, since the numerical coefficient ν_{2T} is given as 50 by Glazman and Matveev.[20] Table II summarizes the determined physical parameters of the localized state in PBCO. The consistency of the parameters listed in Table II was tested by comparing experimentally observed β values in Table I with theoretical ones calculated by Eq. (5) with ν_{3T} which is given by Xu *et al.* as 7.2×10^3.[24] The result is shown in Fig. 9. The agreement between the experiment and the theory is reasonable when one considers the scattering of the experimental data, implying that the parameters in Table I really describe the physical nature of the localized states in PBCO. Further discussion on the consistency of the parameters will be given in the next section concerning the voltage dependence of differential conductance at low temperatures.

C. Voltage dependence of differential conductance

According to the theory proposed by Glazman and Matveev, the voltage dependence of junction conductance due to hopping via a small number of localized states can also be expressed by equations similar to Eq. (5) in which the temperature T is replaced by the voltage V.[20] In the high-bias and low temperature limit $eV \gg k_B T$, the voltage dependence of conductance due to hopping via n localized states $G_n(V)$ is given by

TABLE II. Physical parameters for the localized states in PBCO determined through the comparison between theory and experiments for the temperature dependence of conductance of Au/PBCO/YBCO junctions.

Quantity	Symbol	Units	Value
Density of localized states	g	eV^{-1} cm^{-3}	5×10^{19}
Radius of localized states	a	nm	1.1
Average barrier height	E_0	eV	5.1×10^{-2}
Reduced e-p coupling constant	λ	(dimensionless)	3.4×10^4

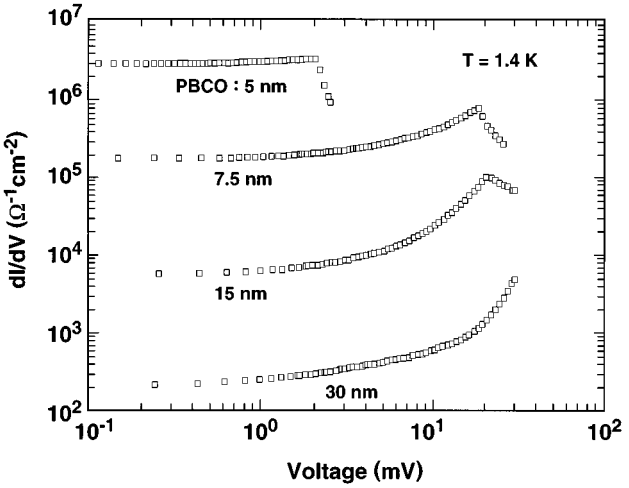

FIG. 10. The differential conductance versus voltage characteristics at 1.4 K in log-log scale for Au/PBCO/YBCO junctions with a PBCO barrier ranging from 5 to 30 nm. The abrupt decrease in the conductance at high voltages which is seen for some junctions is due to the fact that the current flowing in the junctions exceeds the critical current of the bottom YBCO electrodes.

$$G_n(V)=\nu_{nV}\frac{e^2}{\hbar}\,g^n E_0{}^{2/(n+1)}\lambda^{(n-1)/(n+1)}\times(eV)^{(n^2+n-2)/(n+1)}a^{2n-1}d^{n-1}\exp\left(-\frac{2d}{(n+1)a}\right), \tag{14}$$

where V is the voltage and ν_{nV} is a numerical coefficient of which the absolute value has been obtained by Xu *et al.* as $\nu_{nV}\sim(n-1)^{n-1}$.[24] The above expression is for dc conductance, i.e., I/V where I denotes the current. Therefore, the differential conductance $g_n(V)$ is expressed as

$$g_n(V)=\frac{n^2+2n-1}{n+1}\,\nu_{nV}\frac{e^2}{\hbar}\,g^n E_0{}^{2/(n+1)}\lambda^{(n-1)/(n+1)}\times(eV)^{(n^2+n-2)/(n+1)}a^{2n-1}d^{n-1}\exp\left(-\frac{2d}{(n+1)a}\right). \tag{15}$$

In this section, the validity of Eq. (15) is investigated for Au/PBCO/YBCO junctions at 1.4 K within a bias voltage range from 0 to 20–30 mV.

Figure 10 shows the differential conductance versus voltage characteristic at 1.4 K in log-log scale for junctions with a PBCO barrier of various thickness. As the PBCO barrier thickness increases, the Ohmic behavior diminishes at lower voltages and the nonlinear characteristic becomes more pronounced at higher bias voltages. A fundamental problem in analyzing the data in Fig. 10 based on an equation similar to Eq. (9) is how to deal with the contribution from the variable range hopping in a moderately high electric field. Apsley and Hughes have demonstrated that at the limit of high electric field the conductivity due to variable range hopping is essentially independent of temperature and can approximately be described by[25]

$$\sigma=\sigma^* F^{-1/4}\exp(-(F^*/F)^{1/4}), \tag{16}$$

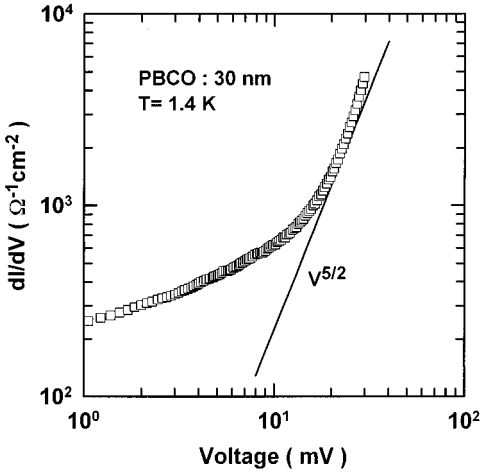

FIG. 11. The log-log plot of the differential conductance versus voltage characteristic at 1.4 K for a junction with a 30-nm thick PBCO barrier. The slope of the curve increases with increasing the voltage, amounting to 5/2 at around 20 mV. This indicates that Eq. (18) can be applied for the fit only below this bias voltage.

where F denotes the electric field and F^* is a characteristic electric field. This simple formula, however, is valid only when the electric field F satisfies the following condition:

$$F\geqslant 10\,\frac{2k_BT}{ea}. \tag{17}$$

In our experimental condition, that is, $T=1.4$ K, Eq. (17) is satisfied when $F>2.2\times10^4$ V/cm. This corresponds to bias voltages of 11 mV and 66 mV for 5-nm thick and 30-nm thick barrier junctions, respectively. Unfortunately, we were not able to apply these high bias voltages to our junctions because the current flowing in the junction exceeded the critical current of the bottom YBCO electrodes. On the other hand, the general formula given by Apsley and Hughes for the conductivity due to variable range hopping in arbitrary electric field is too complicated to apply directly to the analysis of the experimental data. Thus, in the present work we restricted ourselves to analyze the data obtained at relatively low bias voltages using an equation which contains only the terms corresponding to hopping conduction via up to three localized states:

$$dI/dV=g_0+\alpha_V V^{4/3}+\beta_V V^{5/2}, \tag{18}$$

where g_0 describes the differential conductance which comes from tunneling processes, and α_V and β_V denote fitting parameters for hopping conduction via two and three localized states, respectively. We assumed that g_0 was independent of voltage within the bias conditions that we used in our experiment. The fitting procedure started with the determination of the voltage region to be used for fitting the experimental data for individual junctions by plotting the differential conductance versus voltage characteristic in log-log scale. Figure 11 shows an example of the plot for a 30-nm thick barrier junction. In the case of this junction, the slope of the curve reaches 5/2 at around the bias voltage of 20 mV. This indicates that Eq. (18) can be appalied only below this bias voltage. Such a restriction of voltage region used for fitting was not necessary for junctions with a PBCO barrier thinner than

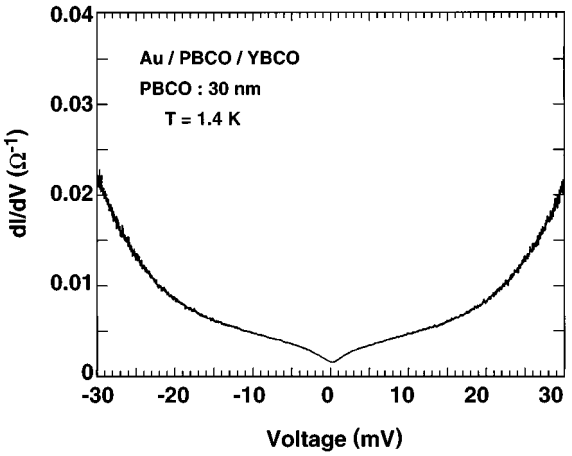

FIG. 12. The plot of the differential conductance versus voltage characteristic at 1.4 K in linear scale for a junction with a 30-nm thick PBCO barrier. A symmetrical dip with its minimum at zero voltage is seen below 5 mV, which is definitely out of the scope of simple tunneling and hopping conduction models.

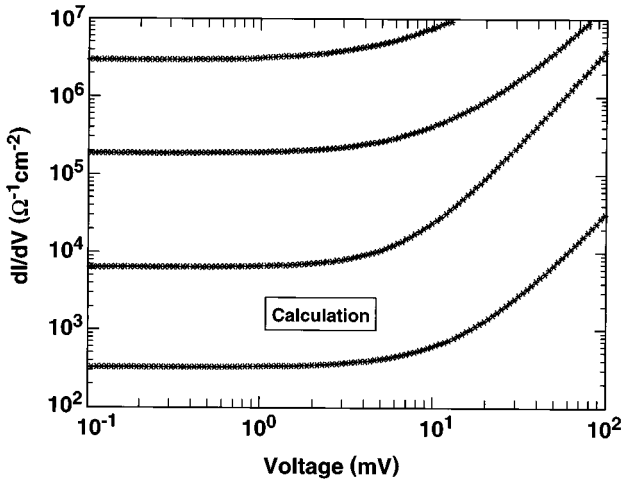

FIG. 13. Theoretical voltage dependence of differential conductance calculated by Eq. (18) and numerical parameters listed in Table II. Each curve in the figure corresponds to the experimental data for junctions with a PBCO barrier of various thickness shown in Fig. 10.

10 nm, for which the slope of $\log(dI/dV)$ versus $\log V$ curves never reached 5/2 up to the bias voltage where the bottom YBCO layer turned into the normal state. Another restriction of the bias voltage region was required for some junctions in the lower voltage region because of the presence of an anomalous behavior around zero voltage. Figure 12 shows the dI/dV versus V characteristic in linear scale for a 30-nm thick barrier junction. A symmetrical dip with its minimum at zero voltage is clearly seen. Although a similar conductance dip was more or less observed for all the junctions except one with a 5-nm thick PBCO barrier, it seemed to be enhanced with an increase in the PBCO barrier thickness. We shall return to this point later in this section. It is apparent that such a dip structure in dI/dV profiles would not be expected from Eq. (18), and so the fits were restricted to above 1 and 5 mV for 20-nm thick and 30-nm thick PBCO barrier junctions, respectively. For other junctions, fitting was performed from zero voltage because the zero-bias anomaly was not thought to influence the fitting significantly.

Table III summarizes the parameters in Eq. (18) obtained by the fit, in which two values in each column represent the values corresponding to either positive or negative bias condition. The reproduced dI/dV characteristics corresponding to Fig. 10 are shown in Fig. 13. The overall agreement between Fig. 10 and Fig. 13 is satisfactory, implying that Eq. (18) describes the behavior of dI/dV versus V characteristic well, at least in moderate voltage regions. In order to see whether the parameters tabulated in Table III are consistent with those in Table I or not, we performed the theoretical calculation of α_V and β_V using Eq. (15) and physical parameters listed in Table II, and compared the results with the experiment. Figures 14 and 15 compare the experimental α_V and β_V values with the theoretical estimation. The agreement between the experimental data and the theory is fairly good in both cases, indicating that the physical parameters in Table II which were derived from the conductance versus temperature characteristics can also account for the conductance versus voltage characteristics.

The remaining problem respecting the dI/dV versus V characteristics of our junctions is the zero-bias anomaly for which we have already presented one example in Fig. 12. The difference between G_0 in Table I and g_0 in Table III expresses the measure of the anomaly for all the junctions which we have investigated. We recognized that the zero -bias anomaly tended to be enhanced with increasing the PBCO barrier thickness. Figure 16 shows the dI/dV data at 1.4 K as a function of $V^{4/3}$ for a junction with a 7.5-nm thick PBCO barrier. It can be recognized that although the differential conductance exhibits a nearly linear dependence on $V^{4/3}$ at low voltages, it decreases more rapidly below 2 mV. This slight decrease in the dI/dV values around zero voltage corresponds to the zero bias anomaly which becomes clearer

TABLE III. Parameters for Eq. (18) obtained by the fits to the experimental differential conductance versus voltage characteristics shown in Fig. 10.

d (nm)	g_0 (Ω^{-1} cm^{-2})	α_V (Ω^{-1} cm^{-2} mV$^{-4/3}$)	β_V (Ω^{-1} cm^{-2} mV$^{-5/2}$)
5	2.9×10^{6}	$2.1–2.3\times10^{5}$	
7.5	1.8×10^{5}	$0.98–1.04\times10^{4}$	$0.1–1.1\times10^{2}$
10	5.5×10^{4}	$5.1–5.2\times10^{3}$	$3.4–4.0\times10^{2}$
15	5.7×10^{3}	$4.9–6.3\times10^{2}$	$1.4–2.2\times10^{1}$
20	1.1×10^{3}	$8.8–8.9\times10^{1}$	$5.4–5.5\times10^{0}$
30	$2.9–3.4\times10^{2}$	$1.0–1.5\times10^{1}$	$1.8–2.7\times10^{-1}$

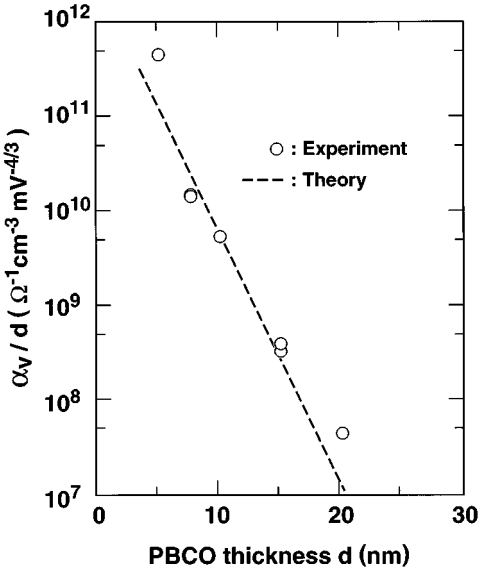

FIG. 14. Comparison between experimentally determined coefficients of the $V^{4/3}$ term in differential conductance (open circles) and theoretical calculation (dashed line) using Eq. (15) and physical parameters for the localized states in PBCO listed in Table II.

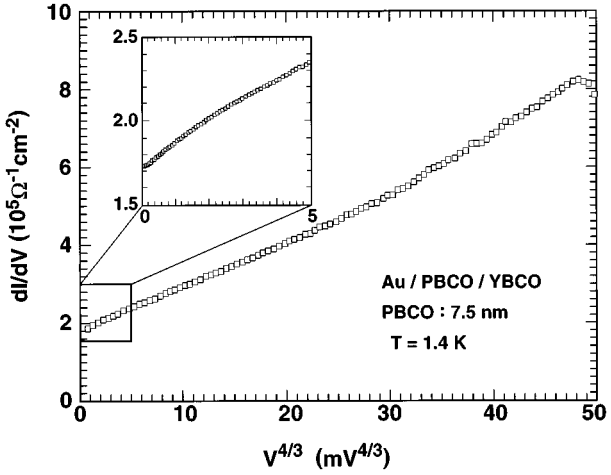

FIG. 16. Plot of the differential conductance dI/dV of a junction with a PBCO barrier of 7.5 nm in thickness as the function of the 4/3 power of voltage V. The differential conductance obeys the $V^{4/3}$ law at low voltages except in the close vicinity of zero voltage. The slight decrease in the differential conductance below 2 mV, which can be clearly seen in the magnified figure, corresponds to the zero-bias anomaly which becomes clearer for thicker barrier junctions.

for thicker barrier junctions, as typically shown in Fig. 12 for a 30-nm thick barrier junction.

In our previous paper, we reported that conductance dip similar to that in Fig. 12 was observed for YBCO/PBCO/YBCO junctions with a PBCO barrier layer thicker than 20 nm at low temperatures, and argued that one possible explanation for the anomaly might be a quantum correction of the density of states in a disordered metal region formed in the vicinity of the interface between the barrier and electrodes.[17] In fact, a theoretical calculation based on the quantum correction model by Al'tshuler and Aronov[26] has given a semiquantitative agreement with the dI/dV profiles. The quantum correction model, however, cannot account for the barrier thickness dependence of the zero-bias anomaly observed in the present work. The anomaly differs also from that observed for some junctions with an amorphous Si barrier,[24] for which the anomaly decreases with an increase in the barrier layer thickness. Although a satisfactory explanation has not been obtained yet for the origin of the zero-bias anomaly in junctions with a PBCO barrier, we can probably rule out the possibility of a magnetic origin because a high magnetic field up to 6 T had negligible effects on the conductance dip in YBCO/PBCO/YBCO junctions.[17] One plausible explanation for the anomaly may be a charging effect in resonant tunneling of electrons through two or more consecutive localized states which are aligned with each other in energy as well as in space. It is known that such a resonant tunneling process exhibits the same thickness dependence as the ordinary resonant tunneling and is non-negligible for a junction with a thick barrier.[22] It may not be difficult to suppose that the Coulomb interaction between electrons at different resonant states partially suppresses the tunneling probability at low voltages in a similar way that the Coulomb interaction leads to a gap in the density of localized states in the variable range hopping regime.[27] More work, however, is needed to clarify the origin of the zero-bias anomaly in our junctions.

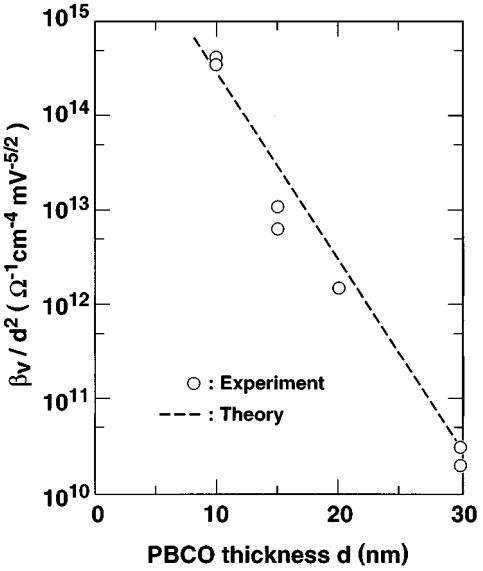

FIG. 15. Comparison between experimentally determined coefficients of the $V^{5/2}$ term in differential conductance (open circles) and theoretical calculation (dashed line) using Eq. (5) and physical parameters for the localized sates in PBCO listed in Table II.

D. Magnetic field effect on junction conductance

In the process of resonant tunneling, an electron passing through the resonant state is regarded as staying at the state during the tunneling time which is inversely proportional to the tunneling width. As a result, the Coulomb repulsion between electrons which tunnel through one localized state becomes appreciable, resulting in a strong suppression of resonant tunneling of Cooper pairs. The role of the Coulomb interaction in resonant tunneling of Cooper pairs has been investigated theoretically by Glazman and Matveev.[28] Ac-

cording to their theory, the manner in which the possibility of resonant tunneling of Cooper pairs is considered has to differ depending on the relative amplitude of two time scales: electron tunneling time $\hbar/\Gamma$ and the correlation time of the electrons in a Cooper pair $\hbar/k_BT_c$, where T_c denotes the transition temperature of superconductive electrodes. In the case of $\Gamma < k_BT_c$, simultaneous tunneling of two electrons in a pair is required to sustain resonant Josephson current. The Coulomb repulsion U at the localized states usually prohibits such a process, resulting in a strong suppression of the Josephson current. On the other hand, if Γ is larger than k_BT_c, two electrons in a pair can tunnel through the barrier separately in time without the loss of the pair correlation. In such a case, the Josephson current does not suffer a suppression due to the Coulomb repulsion, or it may even be enhanced owing to the formation of a collective Kondo resonance state at the Fermi level. In the case of our junctions, Γ can be estimated to be 5.5 μeV for a 7.5-nm thick barrier junction from the physical parameters listed in Table II. Since the Coulomb repulsion energy at the localized state is expressed as $U \approx e^2/\varepsilon a$, the value exceeds 160 meV even if we assume a large dielectric constant amounting to 100 in PBCO. Thus the condition $U \gg k_BT_c \gg \Gamma$ is satisfied in our experiments. The Josephson critical current density at zero temperature under this condition is given by

$$J_c \approx \frac{e}{\hbar} E_0^2 g\left(d - a \ln\frac{E_0}{\Delta}\right)\exp\left(-\frac{2d}{a}\right), \tag{19}$$

where Δ is the superconductive gap energy of the electrodes. A numerical calculation of Eq. (19) with the parameters listed in Table II yields 0.3 A/cm^2 for a YBCO/PBCO/YBCO junction with a 10-nm thick barrier. This value is several orders of magnitude smaller than that observed for ramp-edge-type junctions[6,7,14] as well as for sandwich-type junctions.[17]

The preliminary consideration described above seems to deny the possibility of resonant tunneling of Cooper pairs in YBCO/PBCO/YBCO junctions unless we assume an anomalously weak Coulomb repulsion at the localized states in PBCO. The effect of Coulomb repulsion at localized states on resonant tunneling of single electron has been investigated by Glazman and Matveev under the conditions $U \gg T \gg \Gamma$.[29] They have shown that even above the Kondo temperature of the resonant tunneling system, the Coulomb interaction in the localized states manifests itself in the line shape of the resonant energy level, resulting in a modification of tunneling current from that expected for a system without the interaction. The most striking consequence of the Coulomb interaction is that the resonant tunnel conductance exhibits a characteristic dependence on a magnetic field. In the case that a tunneling barrier contains a large number of localized states with a uniform distribution the conductance averaged over the position and energy of the localized states in the magnetic field B is given by

$$G(B) = \frac{\pi e^2}{\hbar} ga\Gamma F\left(\frac{\mu_B B}{k_B T}\right), \tag{20}$$

$$F(x) = e^{2x}\ln(1+e^{-2x}) + e^{-2x}\ln(1+e^{2x}), \tag{21}$$

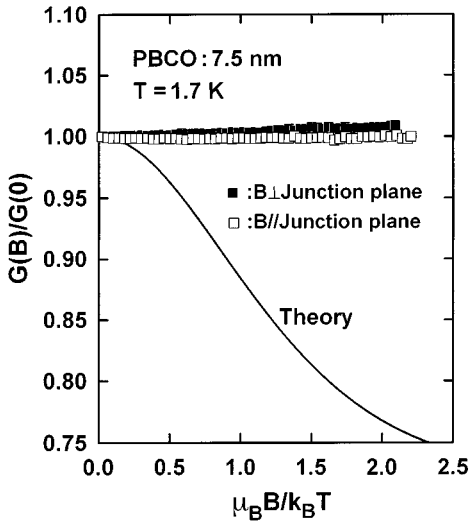

FIG. 17. Magnetic field dependence of the normalized zero-voltage conductance at 1.7 K for a junction with a 7.5-nm thick PBCO barrier. The solid squares show the data observed in a magnetic field perpendicular to the junction plane and the open squares correspond to the data in a magnetic field parallel to the junction plane. The solid line shows the theoretical prediction for resonant tunneling via a spin-degenerate localized state with a large on-site Coulomb repulsion between electrons.

where μ_B denotes the Bohr magneton. It should be noted that at the limit of high magnetic field, Eq. (20) coincides with the formula for resonant tunneling without an inclusion of the Coulomb repulsion effect. This can be understood as the result of the freezing out of the spin-flip tunneling process in a strong magnetic field.

The magnetic field effect described by Eqs. (20) and (21) has been confirmed experimentally for Mo/amorphous Si/Mo junctions by Ephron *et al.*[30] We performed a similar experiment for our Au/PBCO/YBCO junctions in order to investigate whether a similar effect existed in the junctions or not. We selected junctions with a PBCO barrier thinner than 10 nm for which resonant tunneling was confirmed unambiguously to dominate the current conduction at low temperatures. The zero-bias anomaly discussed in the preceding section was negligible for these junctions. Figure 17 shows the zero-voltage conductance of a 7.5-nm thick barrier junction at 1.7 K as a function of magnetic field which was directed either perpendicular or parallel to the junction plane. Theoretical dependence calculated from Eq. (20) and (21) is also shown in the figure. It is apparent that the magnetic field has a negligible effect on the junction conductance, which forms a striking contrast to the theory. All the junctions that we have investigated exhibited a similar behavior.

The experimental result shown in Fig. 17 indicates clearly that the theory of Glazman and Matveev cannot be applied to our junctions. One possible explanation for this discrepancy may be that the Coulomb repulsion at the localized states in PBCO is anomalously weakened for some reasons. If this is actually the case, we can expect resonant tunneling of Cooper pairs in Josephson junctions with a PBCO barrier. Such a situation, however, requires quite an anomalous electronic state of the localized states in PBCO. Although a negative U center at which an attractive interaction exists between electrons is a possible candidate,[8] we do not have any direct

evidence to support the possibility. A more plausible explanation for the behavior of our junctions is that the precondition which makes Eq. (20) and (21) valid is not satisfied in PBCO. Ng and Lee have discussed that the coupling of the resonant state with other localized states has a great influence on the Coulomb correlation effect on resonant tunneling.[31] The magnetic moments on singly occupied localized states separated by distance l are known to interact via an antiferromagnetic exchange $J \propto \exp(-l/a)$ and form a spin singlet when J exceeds $k_B T$. Such an interaction is definitely out of the scope of the theory of Glazman and Matveev. It is easy to suppose that the applied magnetic field has little effect on resonant tunneling of electrons as long as $\mu_B B$ is far smaller than J, because spin-flip tunneling is already suppressed by the exchange interaction between localized moments.

IV. SUMMARY AND CONCLUSION

We have presented a detailed investigation of the mechanism of current transport across thin PBCO barrier layers in a,b-axis oriented Au/PBCO/YBCO junctions. Characteristic power-law dependence of junction conductance was confirmed at low temperatures for junctions with a PBCO barrier thinner than 30 nm, indicating that resonant tunneling and hopping transport through a small number of localized states were predominant. The hopping conduction via a small number of localized states was found to cross over fairly abruptly to variable range hopping when both the barrier thickness and temperature were increased. Least squares fitting of the experimental data to the equation based on the theory of Glazman and Matveev[20] enabled us to determine the physical parameters concerning the localized states in PBCO. We have concluded that the localized states in PBCO have a radius of around 1.1 nm and are populated with a density of states of 5.0×10^{19} $\mathrm{eV}^{-1}\,\mathrm{cm}^{-3}$. The effective depth and the electron-phonon coupling parameter of the localized states have also been derived.

The differential conductance of the junctions at low temperatures also exhibited a power-law dependence on the bias voltage unless the bias was not too high. We have demonstrated that the voltage dependence was quantitatively explained by the theory of Glazman and Matveev when we adopted the physical parameters of the localized states derived from the temperature dependence of junction conductance. On the other hand, most of the junctions exhibited a zero-bias anomaly in their dI/dV profiles which is definitely out of the scope of Glazman and Matveev's model. This anomaly tended to be enhanced with an increase in the PBCO barrier thickness, implying that it may be related with some charging effect associated with the localized states. The origin of this anomaly, however, is not fully understood.

The most striking contrast of our results to those reported for amorphous Si barrier[30] is that we have not been able to observe any decrease of the junction conductance with an applied magnetic field in the resonant tunneling regime. We can conceive two possible explanations for our experimental result. One is that the Coulomb repulsion between electrons at the localized states is screened to nearly zero or is even attractive due to some anomalous mechanism. Another possibility which is more plausible is that antiferromagnetic exchange coupling occurs between the singly occupied localized states.[31] It is highly probable that the exchange coupling already suppresses the spin-flip tunneling of electrons in zero magnetic field, resulting in the insensitivity of junction conductance to the applied magnetic field.

The radius of the localized states in PBCO which we have derived in the present investigation is far smaller that those estimated in YBCO/PBCO/YBCO junctions.[6,7,10,14] This discrepancy may be attributed to the difference in the junction structures. It is probable that the potential barrier in our junctions has an asymmetric shape originating inherently from the asymmetric configuration of the electrodes. The difference in work functions between Au and YBCO or in the interface structure between Au/PBCO and PBCO/YBCO may result in a builtin field in the barrier, which raises the effective barrier height near the Au/PBCO interface. Such a picture seems to be consistent with the fact that the thickness dependence of the conductance due to resonant tunneling becomes weaker with increasing the PBCO layer thickness. We also notice that the Au/PBCO/YBCO junctions always exhibit a lower conductance than YBCO/PBCO/YBCO junctions with the same PBCO barrier thickness.[17] This also supports the asymmetric barrier model for Au/PBCO/YBCO junctions.

ACKNOWLEDGMENT

This work was performed under the management of the R&D Association for Future Electron Devices as a part of the R&D of Basic Technology for Future Industries supported by the New Energy and Industrial Technology Development Organization.

[1] K. K. Likharev and V. K. Semenov, IEEE Trans. Appl. Supercond. **1**, 3 (1993).

[2] T. Hashimoto, M. Sagoi, Y. Mizutani, J. Yoshida, and K. Mizushima, Appl. Phys. Lett. **60**, 1756 (1992).

[3] T. Umezawa, D. J. Lew, S. K. Streiffer, and M. R. Beasley, Appl. Phys. Lett. **63**, 3221 (1993).

[4] H. Sato, H. Akoh, and S. Takada, Appl. Phys. Lett. **64**, 1286 (1994).

[5] Yu. M. Boguslavskij, J. Gao, A. J. H. M. Rijnders, D. Terpstra, G. J. Gerritsma, and H. Rogalla, Physica C **194**, 268 (1992).

[6] Y. Sawada, H. Terai, A. Fujimaki, Y. Takai, and H. Hayakawa, IEEE Trans. Appl. Supercond. **5**, 2099 (1995).

[7] T. Satoh, M. Yu. Kupriyanov, J. S. Tsai, M. Hidaka, and H. Tsuge, IEEE Trans. Appl. Supercond. **5**, 2612 (1995).

[8] J. Halbritter, Phys. Rev. B **46**, 14 861 (1992).

[9] I. A. Devyatov and M. Yu. Kupriyanov, JETP Lett. **59**, 200 (1994).

[10] A. A. Golubov, M. A. J. Verhoeven, I. A. Devyatov, M. Yu. Kupriyanov, G. J. Gerritsma, and H. Rogalla, Physica C **235-240**, 3261 (1994).

[11] R. Fehrenbacher and T. M. Rice, Phys. Rev. Lett. **70**, 3471 (1993).
[12] K. Takenaka, Y. Imanaka, K. Tamasaku, T. Itoh, and S. Uchida, Phys. Rev. B **46**, 5833 (1992).
[13] L. Hoffman, A. A. Manuel, M. Peter, E. Walker, M. Ganthier, A. Shukla, B. Barbiellini, S. Massidda, Gh. Adam, S. Adam. W. N. Hardy, and Ruixing Liang, Phys. Rev. Lett. **71**, 4047 (1993).
[14] M. A. Verhoeven, G. J. Gerritsma, H. Rogalla, and A. A. Golubov, Appl. Phys. Lett. **69**, 848 (1996).
[15] M. Lee, Y. Suzuki, and T. H. Geballe, Phys. Rev. B **51**, 15 619 (1995).
[16] H. A. Blackstead, J. D. Dow, D. B. Chrsey, J. S. Horwitz, M. A. Black, P. J. McGinn, A. E. Klunzinger, and D. B. Pulling, Phys. Rev. B **54**, 6122 (1996).
[17] J. Yoshida, T. Nagano, and T. Hashimoto, Phys. Rev. B **53**, 8623 (1996).
[18] J. Yoshida, T. Hashimoto, S. Inoue, Y. Mizutani, M. Sagoi, and K. Mizushima, Jpn. J. Appl. Phys. **31**, 1771 (1992).
[19] T. Nagano, T. Hashimoto, and J. Yoshida, Physica C **265**, 214 (1996).
[20] L. I. Glazman and K. A. Matveev, Sov. Phys. JETP **67**, 1276 (1988).
[21] S. J. Bending and M. R. Beasley, Phys. Rev. Lett. **55**, 324 (1985).
[22] A. I. Larkin and K. A. Matveev, Sov. Phys. JETP **66**, 580 (1987).
[23] L. I. Glazman and R. I. Shekhter, Sov. Phys. JETP **67**, 163 (1988).
[24] Y. Xu, D. Ephron, and M. R. Beasley, Phys. Rev. B **52**, 2843 (1995).
[25] N. Apsley and H. P. Hughes, Philos. Mag. **31**, 1327 (1975).
[26] B. L. Al'tshuler and A. G. Aronov, in *Electron-Electron Interactions in Disordered Systems*, edited by A. L. Efros and M. Pollak (North-Holland, Amsterdam, 1985), Chap. 1.
[27] A. L. Efros and B. I. Shklovskii, in *Electron-Electron Interactions in Disordered Systems* (Ref. 26), Chap. 5.
[28] L. I. Glazman and K. A. Matveev, JETP Lett. **49**, 659 (1988).
[29] L. I. Glazman and K. A. Matveev, JETP Lett. **48**, 445 (1988).
[30] D. Ephron, Y. Xu, and M. R. Beasley, Phys. Rev. Lett. **69**, 3112 (1992).
[31] T. K. Ng and P. A. Lee, Phys. Rev. Lett. **61**, 1768 (1988).